International Journal of Control, Automation, and Systems 22(X) (2024) 1-14
http://dx.doi.org/10.1007/s12555-023-0424-5
ISSN:1598-6446 eISSN:2005-4092
http://www.springer.com/12555

The Dynamical Model and the Slithering Controller of Continuous Snake-like Robot on Smooth Surface

Koki Harada, Ryo Ariizumi*, Toru Asai, and Shun-ichi Azuma

Abstract: This paper introduces a new dynamical model for a continuous snake-like robot and a controller yielding slithering motion on a smooth curved surface. Smooth curve models are common tools in studies on snake-like robots, however, the application of those models is limited to cases without sideslips. Our new model can deal with locomotion with sideslips on curved surfaces. Moreover, the numerical simulation of climbing up the surface of a cylinder based on our model reveals the important role of the tangential friction of the body, which was underestimated by previous studies. The result illuminates the trade-off relation between the energy efficiency and the reachability of the snake-like robots.

Keywords: Control, distributed parameter model, locomotion on manifold, snake-like robot.

NOMENCLATURE

t	The time
σ	The arc-length parameter
$\boldsymbol{x}(\sigma,t)$	The position of the body segment at (σ,t)
$\{\boldsymbol{e}_r,\boldsymbol{e}_p,\boldsymbol{e}_y\}$	The backbone frame along the curve $\boldsymbol{x}$
$\{\boldsymbol{e}_r,\boldsymbol{e}_b,\boldsymbol{e}_n\}$	The Darboux frame along the curve $\boldsymbol{x}$
$\boldsymbol{\omega}_{bc}(\sigma,t)$	The angular velocity of the backbone frame at (σ,t) with respect to itself
$\boldsymbol{\omega}_d(\sigma,t)$	The angular velocity of the backbone frame at (σ,t) with respect to $\{\boldsymbol{e}_r(\sigma,t),\boldsymbol{e}_b(\sigma,t),\boldsymbol{e}_n(\sigma,t)\}$
$\tilde{\boldsymbol{\omega}}_d(\sigma,t)$	The angular velocity of the Darboux frame at (σ,t) with respect to itself
$\begin{bmatrix}\omega_r(\sigma,t)\\ \omega_p(\sigma,t)\\ \omega_y(\sigma,t)\end{bmatrix}$	The components of $\boldsymbol{\omega}_{bc}(\sigma,t)$
$\begin{bmatrix}\omega_r(\sigma,t)\\ \omega_b(\sigma,t)\\ \omega_n(\sigma,t)\end{bmatrix}$	The components of $\boldsymbol{\omega}_d(\sigma,t)$
$\begin{bmatrix}\tilde{\omega}_r(\sigma,t)\\ \tilde{\omega}_b(\sigma,t)\\ \tilde{\omega}_n(\sigma,t)\end{bmatrix}$	The components of $\tilde{\boldsymbol{\omega}}_d(\sigma,t)$

1. INTRODUCTION

Snakes have notable performance in locomotion. The legless creatures can slither on various terrains such as tree branches or rocky fields by fitting their bodies onto the surfaces. The high mobility on various terrains and the stability on the surfaces have induced research on snake-like robots [1,2]. These robots are expected to be useful in rescue missions, for example.

Typical snake-like robots consist of serially connected joints to imitate living snakes. The numerous joints make it valid to regard a snake-like robot as a smooth curve. Expressing the body shape and orientation of a snake-like robot as a smooth curve and a moving frame on it has been popular in gait design research [2-5].

The smooth curve model approach is also used in the mechanical analysis of snake-like robots. Yamada and Hirose [6] studied the relationship between friction, internal force, and input torque on a snake. They gave significant insight into the slithering and sprinting gaits, also known as the sinus-lifting gait. Date and Takita [7] worked on an optimal control law for a snake-like robot based on a smooth curve dynamic model. They also discretized the proposed controller and examined its efficacy using a real snake-like robot. Ha [8] focused on the compliance of the continuous snake-like robots. He revealed that lateral undulatory locomotion with simple tension control spontaneously yields various gaits presented in the previous stud-

Manuscript received July 3, 2023; revised February 20, 2024; accepted June 19, 2024. Recommended by Associate Editor Jongho Lee under the direction of Senior Editor Dongjun Lee. This research was supported by JSPS KAKENHI JP18K04011 and JP21H01285.

Koki Harada is with the Department of Mechanical Systems Engineering, Nagoya University, Furo-cho, Nagoya, Japan (e-mail: harada.koki.s8@s.mail.nagoya-u.ac.jp). Ryo Ariizumi is with the Department of Mechanical Systems Engineering, Tokyo University of Agriculture and Technology, Tokyo 184-8588, Japan (e-mail: ryoariizumi@go.tuat.ac.jp). Toru Asai is with the the Department of Mechanical Engineering, Chubu University, Aichi 487-8501, Japan (e-mail: toru.asai@fsc.chubu.ac.jp). Shun-ichi Azuma is with the Graduate School of Informatics, Kyoto University, Kyoto 606-8501, Japan (azuma.shunichi.3e@kyoto-u.ac.jp).
* Corresponding author.

ies. Travers *et al*. [9] and Rollinson *et al*. [10] also took notice of the compliance. Travers *et al*. proposed the adaptive control technique to unknown terrains based on the compliance of the parameters of the desired shape of the robot written as a smooth curve. Rollinson *et al*. proposed the gait that simultaneously achieves locomotion and adaptation of the robot shape to 3D terrains including the human body.

The smooth curve model is often employed in soft-robotics. Mochiyama [11] proposed an approach for the system theory of soft elastic rods. In his study, he utilized the smooth curve theory closely related to the smooth curve model of the snake-like robot. Xun *et al*. [12] modeled complex dynamics of soft slender robots including collision. In their framework, the Cosserat-rod model plays the major role, where the smooth curve model forms the foundation. Gazzola *et al*. [13] and Zhang *et al*. [14] examined snake locomotion on a flat plane as a test problem of their dynamical models for a filament. They implemented simple models for muscle of a snake and successfully generated lateral undulation of a snake by activating its muscle.

One of the common assumptions on the models of the snake-like robots of the previous studies was the absence of sideslips [6-8,15-17]. However, in many practical situations, the validity of this assumption is questionable. Ma [18] exemplified that snake-like robots always sideslipped when they slithered. From our past experiments, a wheeled snake-like robot sideslipped even though it was equipped with rubber wheels and slithered on a mat to achieve a high friction coefficient. Thus, it is also a common assumption that a snake-like robot can sideslip and assume viscous friction [19-22] when using a multilink model.

Applying the viscous friction model to the smooth curve model also seems to be a natural idea. However, this change requires a completely different scheme to determine the motion of the robot from the existing ones. The difficulty lies in the determination of internal forces. In the case of the multilink model, the internal forces can be obtained and removed from the equation of motion by a simple algebraic calculation. However, some of the linear equations in the case of a multilink model can correspond to partial differential equations in the case of a smooth curve model. Thus, such an algebraic technique is sometimes not sufficient to remove or calculate the internal forces. Yamada and Hirose [6] handled the internal force distribution in their work, and Date and Takita [7] derived a method to eliminate the internal forces from the equation of motion. Though, their methods are not directly applicable under viscous friction; the assumption that the robot does not sideslip is a critical factor for their methods. Our research focuses on the determination problem of the internal force distribution and develops a new smooth curve dynamic model that can describe much wider locomotion.

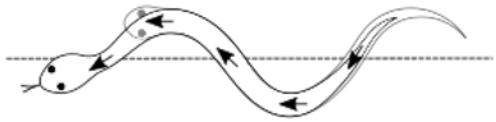

(a) The admissible velocity of the related studies [6,7]. In [6], the body shape also needs to be periodic.

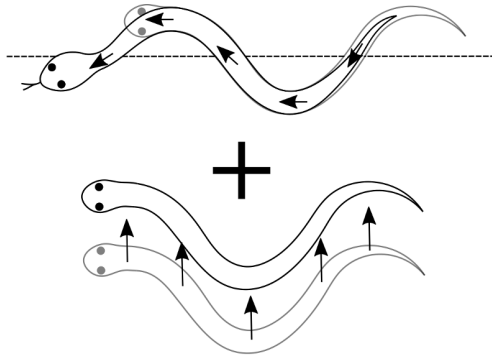

(b) The admissible velocity of this paper. In addition to the admissible velocity of the previous studies, the velocity is allowed in the normal direction of the body axis.

Fig. 1. The difference of the admissible velocity (arrows) between the related studies [6,7] and our study.

This paper consists of 7 sections. Section 2 describes the difference between our study and the previous studies in more detail. Section 3 introduces the kinematics of the continuous snake-like robot. Section 4 describes the dynamical model and the determination problem of the internal force. In Section 5, we derive simple controllers for the continuous robot as an application of our model. The numerical simulation based on our model is illustrated in Section 6, and the conclusions of this paper are given in Section 7.

2. DIFFERENCES FROM THE RELATED STUDIES

Date and Takita [7] dealt with an optimal control law for a continuous snake-like robot that does not sideslip on a smooth surface. Exploiting the constraint on sideslips, he derived a method to calculate the body acceleration from the input torque distribution. Yamada and Hirose [6] worked on the internal force distribution of a continuous snake model with infinite length. Even though they did not deal with the time development of the shape, they derived the equations of equilibrium of forces and torques of the infinitesimal segment of the body, and they gave profound insights into serpentine locomotion and sinus-lifting locomotion, which were common among various

snake species.

Our model shares the basic structure with them. However, there exists a crucial difference that calls for a completely different handling of the internal force distribution of the robot. Though Date and Takita [7] put a constraint on sideslips (Fig. 1(a)), our model allows the segment to do that (Fig. 1(b)). This mitigation originated in real-world snake-like robots. The constraint is a common assumption for wheeled snake-like robots. However, in the real world, the wheels often slip in sideways, and the robots' locomotion fails to match the expectation.

The sideslip can easily be accounted for only by the change in the friction model. However, the loss of the constraint results in a crucial difference. The method in [7] for calculating the acceleration fully depends on the constraint. The constraint forces the acceleration in the tangent direction of the body to be the same everywhere in the body. Therefore, the internal forces of the robot are easily eliminated from the equation of motion by integrating each of the equations of the infinitesimal segments. Without the constraint on sideslips, the calculation of the time development must deal with the internal force distribution. However, the previous study [6] on the internal force distribution cannot be applied directly in our case. Their study assumes the constant frictional force distribution throughout the robot, which is derived from the constraint on sideslips. In addition, the two kinds of locomotion they examined consist of a periodic undulation of the body, which leads to a periodic distribution of the internal force. Their calculation method for the internal force relies on both the constant frictional force distribution and the periodicity, thus the method is not applicable to our model which allows any smooth body shape.

The studies by Gazzola *et al.* [13] and Zhang *et al.* [14] develop the dynamical models for filaments and, as a test for the models, examine the snake locomotion on a flat plane by regarding the snake as a filament. The study by Xun *et al.* [12] does not directly examine snake locomotion, however, they handle similar slender soft robots and examine the dynamics including collision. The models support sideslips, however, also require the elastic properties of the filaments. One of the purposes of the continuous model for snake-like robots is to provide an abstracted model for various snake-like robots including multi-link ones. However, the requirement for the material information restricts the application of the models. In addition, in their numerical simulation, they regard the muscle of the snake as the input. Most snake-like robots use revolutionary motors as their input, thus, the muscle-based input prevents direct application to ordinary snake-like robots.

As [2-8], our continuous model is intended to be an abstraction for snake-like robots including multi-link ones. Thus, the model is constructed without information about any elastic properties. At the same time, as [13,14], our model describes locomotion with sideslips. In addition to the above, the model needs to be applicable to even non-flat terrain. In the following sections, we introduce the novel dynamical model dealing with the problems above.

3. KINEMATICS OF CONTINUOUS SNAKE-LIKE ROBOTS

Most snake-like robots have many joints, which let the robots take various 3-dimensional postures. However, they keep lying on the surface of the terrain during their motion. Therefore, we focus on the locomotion of the robot on a smooth surface in $\mathbb{R}^3$.

3.1. Representation of robot posture

The shape of a curve is described by moving-frame with some form-specifying function, e.g. curvature and torsion for the Frenet-Serret frame. In the previous studies on snake-like robots, they used the backbone frame (the backbone curve) [2-7] to describe both the robot shape and the roll posture in the space. However, considering the constraint on the robot's position, the Darboux frame is suitable to describe the transition of the robot's shape along the surface. The two frames are not identical, and both are used throughout our paper. Therefore, making clear the difference helps in understanding both frames and their role in the paper.

The backbone frame is defined with a curve and a vector field on it. Let the length of the robot be denoted by a constant real positive number L. Then the body curve of the robot is described by a smooth map

$$\boldsymbol{x} : (\sigma, t) \in [0,\ L] \times \mathbb{T} \mapsto \boldsymbol{x}(\sigma, t) \in \mathbb{R}^3, \tag{1}$$

where t is the time, and $\mathbb{T}$ is the time interval we consider. The scalar σ is the arc-length parameter. To describe real-world robots, the curve should have the concept of the back side and the belly side. Defining a smooth vector field $\boldsymbol{e}_y : [0,\ L] \times \mathbb{T} \to \mathbb{R}^3$ on the curve meets the request. More specifically, $\boldsymbol{e}_y(\sigma, t)$ needs to be a unit vector pointing to the direction of the back at $\boldsymbol{x}(\sigma, t)$. As shown in Fig. 2, the body axis of the snake lies in between the belly and the back, thus the vector $\boldsymbol{e}_y(\sigma, t)$ should be orthogonal to the body axis vector $\boldsymbol{e}_r(\sigma, t) := \partial_\sigma \boldsymbol{x}(\sigma, t)$, where $\partial_\sigma \boldsymbol{x}(\sigma, t)$ means the partial derivative of $\boldsymbol{x}(\sigma, t)$ with respect to σ. Similar notation is used for other variables and

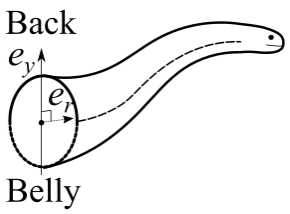

Fig. 2. Belly-back line ($\boldsymbol{e}_y$) and body axis ($\boldsymbol{e}_r$).

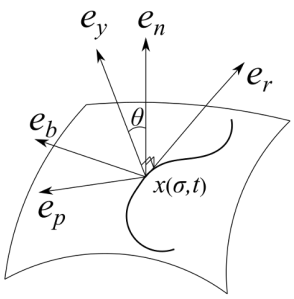

Fig. 3. Directional relationship between Darboux frame and the backbone frame.

higher derivatives. Let us define a unit vector $\boldsymbol{e}_p(\sigma,t)$ by $\boldsymbol{e}_p(\sigma,t) = \boldsymbol{e}_y(\sigma,t) \times \boldsymbol{e}_r(\sigma,t)$. Then the triple $(\boldsymbol{e}_r, \boldsymbol{e}_p, \boldsymbol{e}_y)$ defines a moving frame called the backbone frame along the curve $\boldsymbol{x}$.

On the one hand, the backbone frame is defined only by the curve shape $\boldsymbol{x}$ and the back side indicator $\boldsymbol{e}_y$ without any dependencies on the surrounding space. On the other hand, the Darboux frame depends on $\boldsymbol{x}$ and the surface where the curve lies. Let the two-dimensional smooth surface in $\mathbb{R}^3$ be denoted by S and $\phi : S \to \mathbb{R}^2$ be a local coordinate system of S. In this paper, for the sake of simplicity, it is assumed that S is covered by a single local coordinate chart. In other words, ϕ is a diffeomorphism between S and $\mathbb{R}^2$. Let u, v be local coordinates of S and define a unit vector $\boldsymbol{e}_n(u,v)$ as follows:

$$\boldsymbol{e}_n(u,v) = \frac{\partial_u \phi^{-1}([u,v]^T) \times \partial_v \phi^{-1}([u,v]^T)}{\| \partial_u \phi^{-1}([u,v]^T) \times \partial_v \phi^{-1}([u,v]^T) \|}. \tag{2}$$

This definition makes $\boldsymbol{e}_n(u,v)$ normal to the surface S and also normal to the body axis vector $\boldsymbol{e}_r$ of the robot lying on S. By defining a vector $\boldsymbol{e}_b(\sigma,t)$ by $\boldsymbol{e}_b(\sigma,t) = \boldsymbol{e}_n(\phi(\boldsymbol{x}(\sigma,t))) \times \boldsymbol{e}_r(\sigma,t)$, the triple $(\boldsymbol{e}_r, \boldsymbol{e}_b, \boldsymbol{e}_n)$ becomes the second moving frame on $\boldsymbol{x}$ called the Darboux frame.

As shown in Fig. 3, the two frames share $\boldsymbol{e}_r(\sigma,t)$ and are different from each other by an angle $\theta(\sigma,t)$ around $\boldsymbol{e}_r(\sigma,t)$. The vector field $\boldsymbol{e}_n$ is fixed on the space, thus the angle $\theta(\sigma,t)$ tells the roll orientation of the robot on the surface. The backbone frame tells us the robot's posture on its own without any help from the Darboux frame. However, the position and the velocity of each body segment belong to the tangent bundle TS of S, and the pair $(\boldsymbol{e}_r(\sigma,t),\ \boldsymbol{e}_b(\sigma,t))$ can be identified with a basis of each $T_{\boldsymbol{x}(\sigma,t)}S$. Therefore, the Darboux frame is better suited for the description of the dynamics of the robot.

For the discussion in the following sections, we introduce a property of the Darboux frame and some definitions. Let the vector $\boldsymbol{e}_n(\phi(\boldsymbol{x}(\sigma,t)))$ be abbreviated to $\boldsymbol{e}_n(\sigma,t)$. It is known that differential equations like the Frenet-Serret formulas hold in the case of the Darboux frame

$$\partial_\sigma \boldsymbol{e}_r(\sigma,t) = \kappa_g(\sigma,t)\boldsymbol{e}_b(\sigma,t) + \kappa_n(\sigma,t)\boldsymbol{e}_n(\sigma,t), \tag{3}$$
$$\partial_\sigma \boldsymbol{e}_b(\sigma,t) = -\kappa_g(\sigma,t)\boldsymbol{e}_r(\sigma,t) + \tau_g(\sigma,t)\boldsymbol{e}_n(\sigma,t), \tag{4}$$
$$\partial_\sigma \boldsymbol{e}_n(\sigma,t) = -\kappa_n(\sigma,t)\boldsymbol{e}_r(\sigma,t) - \tau_g(\sigma,t)\boldsymbol{e}_b(\sigma,t). \tag{5}$$

The functions $\tau_g(\sigma,t)$, $\kappa_g(\sigma,t)$, $\kappa_n(\sigma,t)$ are called geodesic torsion, geodesic curvature, and normal curvature, respectively. Note that these functions depend on the partial derivatives of $\boldsymbol{e}_r$, $\boldsymbol{e}_b$, and $\boldsymbol{e}_n$, and the derivations are defined in the open interval $(0,L)$. Therefore, let the values of the functions at $\sigma = 0, L$ be defined by the one-sided derivations of the vectors. Note also that, in this paper, each component of the vectors $\boldsymbol{e}_r(\sigma,t)$, $\boldsymbol{e}_p(\sigma,t)$, $\boldsymbol{e}_y(\sigma,t)$, $\boldsymbol{e}_b(\sigma,t)$, $\boldsymbol{e}_n(\sigma,t)$ is represented in the world frame.

3.2. The velocity constraint on the robot

The constraint that the robot slithers on the surface S also restricts the possible velocity and angular velocity. We introduce the explicit representations of these constraints in this section.

The constraint is described as the following proposition (the definition of $\omega_b(\sigma,t)$ is given later).

Proposition 1: On the surface S, there exist functions $v_r(\sigma,t)$ and $v_b(\sigma,t)$ such that the following equations hold:

$$\partial_t \boldsymbol{x}(\sigma,t) = v_r(\sigma,t)\boldsymbol{e}_r(\sigma,t) + v_b(\sigma,t)\boldsymbol{e}_b(\sigma,t), \tag{6}$$
$$\kappa_n(\sigma,t)v_r(\sigma,t) + \tau_g(\sigma,t)v_b(\sigma,t) + \omega_b(\sigma,t) = 0. \tag{7}$$

The existence of $v_r(\sigma,t)$ and $v_b(\sigma,t)$ and (6) are easy to check. From the assumption, each body segment is bound on the surface. Therefore, the velocity of the segment $\partial_t \boldsymbol{x}(\sigma,t)$ needs to be described by $\boldsymbol{e}_r(\sigma,t)$, $\boldsymbol{e}_b(\sigma,t)$, and some coefficient functions $v_r(\sigma,t)$ and $v_b(\sigma,t)$.

The proof of (7) is slightly complicated. Before deriving the expressions, it is necessary to define the angular velocity of the segment. The dynamics of the robot is discussed on the Darboux frame, however, the frame is independent of the rotational movement of the robot. Instead, the angular velocity must be defined as that of the backbone frame fixed to the segment. Let the angular velocity vector of the backbone frame at (σ,t) with respect to itself be denoted by

$$\boldsymbol{\omega}_{bc}(\sigma,t) = \begin{bmatrix} \omega_r(\sigma,t) & \omega_p(\sigma,t) & \omega_y(\sigma,t) \end{bmatrix}^T. \tag{8}$$

Let $\boldsymbol{\omega}_d(\sigma,t)$ be the Darboux frame representation of the same vector. Thus, by the transformation of the vectors between the frames, $\boldsymbol{\omega}_d(\sigma,t)$ can be described as follows:

$$\boldsymbol{\omega}_d(\sigma,t) := \begin{bmatrix} \omega_r(\sigma,t) \\ \omega_b(\sigma,t) \\ \omega_n(\sigma,t) \end{bmatrix}$$

$$:= R_d(\sigma,t)^T R_b(\sigma,t)\boldsymbol{\omega}_{bc}(\sigma,t), \tag{9}$$

where $R_b(\sigma,t)$ and $R_d(\sigma,t) \in \mathrm{SO}(3)$ are defined as

$$R_b(\sigma,t) = \begin{bmatrix} \boldsymbol{e}_r(\sigma,t) & \boldsymbol{e}_p(\sigma,t) & \boldsymbol{e}_y(\sigma,t) \end{bmatrix}, \tag{10}$$

$$R_d(\sigma,t) = \begin{bmatrix} \boldsymbol{e}_r(\sigma,t) & \boldsymbol{e}_b(\sigma,t) & \boldsymbol{e}_n(\sigma,t) \end{bmatrix}. \tag{11}$$

Equation (7) is derived from the smoothness of the time-variant curve $\boldsymbol{x}$ as follows:

Proof: From (6),

$$\boldsymbol{e}_n(\sigma,t)^T \partial_t \boldsymbol{x}(\sigma,t) = 0, \tag{12}$$

$$\partial_\sigma \boldsymbol{e}_n(\sigma,t)^T \partial_t \boldsymbol{x}(\sigma,t) + \boldsymbol{e}_n(\sigma,t)^T \partial_{\sigma t} \boldsymbol{x}(\sigma,t) = 0, \tag{13}$$

hold. By the smoothness of $\boldsymbol{x}(\sigma,t)$, the partial derivative of $\partial_t \boldsymbol{x}(\sigma,t)$ with respect to σ can be described as follows:

$$\begin{aligned} \partial_{\sigma t}\boldsymbol{x}(\sigma,t) &= \partial_t \boldsymbol{e}_r(\sigma,t) \\ &= (R_b(\sigma,t)\boldsymbol{\omega}_{bc}(\sigma,t)) \times \boldsymbol{e}_r(\sigma,t) \\ &= \omega_y(\sigma,t)\boldsymbol{e}_p(\sigma,t) - \omega_p(\sigma,t)\boldsymbol{e}_y(\sigma,t). \end{aligned} \tag{14}$$

Note that, from (9), $\omega_p(\sigma,t)$, and $\omega_y(\sigma,t)$ can be represented by $\boldsymbol{\omega}_d(\sigma,t)$ as follows:

$$\begin{aligned} \omega_p(\sigma,t) &= \omega_b(\sigma,t)\boldsymbol{e}_b(\sigma,t)^T \boldsymbol{e}_p(\sigma,t) \\ &\quad + \omega_n(\sigma,t)\boldsymbol{e}_n(\sigma,t)^T \boldsymbol{e}_p(\sigma,t), \end{aligned} \tag{15}$$

$$\begin{aligned} \omega_y(\sigma,t) &= \omega_b(\sigma,t)\boldsymbol{e}_b(\sigma,t)^T \boldsymbol{e}_y(\sigma,t) \\ &\quad + \omega_n(\sigma,t)\boldsymbol{e}_n(\sigma,t)^T \boldsymbol{e}_y(\sigma,t). \end{aligned} \tag{16}$$

By substituting (15) and (16) for $\omega_p(\sigma,t)$ and $\omega_y(\sigma,t)$ in (14), $\partial_{\sigma t}\boldsymbol{x}(\sigma,t)$ can be written as follows (we omitted the notation of the variables (σ,t)):

$$\begin{aligned} \partial_{\sigma t}\boldsymbol{x} &= (\omega_b \boldsymbol{e}_b^T \boldsymbol{e}_y + \omega_n \boldsymbol{e}_n^T \boldsymbol{e}_y)\boldsymbol{e}_p - (\omega_b \boldsymbol{e}_b^T \boldsymbol{e}_p + \omega_n \boldsymbol{e}_n^T \boldsymbol{e}_p)\boldsymbol{e}_y \\ &= \omega_b \left((\boldsymbol{e}_b^T \boldsymbol{e}_y)\boldsymbol{e}_p - (\boldsymbol{e}_b^T \boldsymbol{e}_p)\boldsymbol{e}_y \right) \\ &\quad + \omega_n \left((\boldsymbol{e}_n^T \boldsymbol{e}_y)\boldsymbol{e}_p - (\boldsymbol{e}_n^T \boldsymbol{e}_p)\boldsymbol{e}_y \right) \\ &= \omega_b \boldsymbol{e}_b \times (\boldsymbol{e}_p \times \boldsymbol{e}_y) + \omega_n \boldsymbol{e}_n \times (\boldsymbol{e}_p \times \boldsymbol{e}_y) \\ &= -\omega_b \boldsymbol{e}_n + \omega_n \boldsymbol{e}_b. \end{aligned} \tag{17}$$

By substituting (5), (6), and (17) into (13), we get the angular velocity constraint:

$$\kappa_n(\sigma,t)v_r(\sigma,t) + \tau_g(\sigma,t)v_b(\sigma,t) + \omega_b(\sigma,t) = 0. \tag{18}$$

□

Equations (6) and (7) are the velocity constraints on the robot, which tells the robot locomotion consists of two-dimensional translation, rolling movement, and yawing on the surface.

Let $\tilde{\boldsymbol{\omega}}_d(\sigma,t)$ be the angular velocity vector of the Darboux frame written in the Darboux frame, and $\tilde{\omega}_r(\sigma,t)$, $\tilde{\omega}_b(\sigma,t)$, $\tilde{\omega}_n(\sigma,t)$ be the components of $\tilde{\boldsymbol{\omega}}_d(\sigma,t)$, i.e.,

$$\tilde{\boldsymbol{\omega}}_d(\sigma,t) = [\tilde{\omega}_r(\sigma,t), \tilde{\omega}_b(\sigma,t), \tilde{\omega}_n(\sigma,t)]^T. \tag{19}$$

Then, the proof of (7) yields the following corollary:

Corollary 1:

$$\tilde{\omega}_b(\sigma,t) = \omega_b(\sigma,t), \tag{20}$$

$$\tilde{\omega}_n(\sigma,t) = \omega_n(\sigma,t). \tag{21}$$

Proof: The Darboux frame and the backbone frame share $\boldsymbol{e}_r(\sigma,t)$, therefore the time-derivative of $\boldsymbol{e}_r(\sigma,t)$ can also be written as

$$\partial_t \boldsymbol{e}_r(\sigma,t) = \tilde{\omega}_n(\sigma,t)\boldsymbol{e}_b(\sigma,t) - \tilde{\omega}_b(\sigma,t)\boldsymbol{e}_n(\sigma,t). \tag{22}$$

By comparing this equation with (17), the corollary is derived. □

From these equations, we can conclude that the only difference between the angular velocity of the Darboux frame and that of the backbone frame is in the rolling on the surface.

4. DYNAMICS OF CONTINUOUS SNAKE-LIKE ROBOTS

As mentioned in the previous section, the essential motion of the robot segment is classified into three—two-dimensional translation, rolling, and yawing on the surface. Our goal is to derive the equations of motion for these three movements and the method to deal with their time development.

4.1. The forces on the infinitesimal segment

The forces on the segment are classified into gravity, frictional forces, internal force, and constraint force to keep the robot on the surface. As in the previous study [7], let the segment have the length $d\sigma$ and the density ρ. Then we derive the force distribution on the infinitesimal segment by taking the limit as $d\sigma \to 0$.

Let us denote the gravitational acceleration vector as $\boldsymbol{g}$, then the gravitational force on the segment is represented as $\rho d\sigma \boldsymbol{g}$.

To allow the robot to sideslip, we chose the viscous friction model for the frictional forces. The friction force vector $\boldsymbol{f}_{\mathrm{fric}}(\sigma,t)$ is defined as follows:

$$\begin{aligned} \boldsymbol{f}_{\mathrm{fric}}(\sigma,t) &= -c_r d\sigma v_r(\sigma,t)\boldsymbol{e}_r(\sigma,t) \\ &\quad - c_b d\sigma v_b(\sigma,t)\boldsymbol{e}_b(\sigma,t). \end{aligned} \tag{23}$$

In the above definition, the constants $c_r d\sigma$ and $c_b d\sigma$ stand for the viscous coefficient in the tangential and normal directions of the body, respectively. Directional anisotropy of the friction is a critical factor for the slithering locomotion of snake-like robots [19], and is a common assumption for slithering snake-like robots [19-22]. Therefore, we also assume the frictional anisotropy i.e., $c_r < c_b$ in the present paper.

The internal forces act on both ends of the segment. Let the internal force distribution be denoted by $\boldsymbol{F} : [0, L] \times$

$\mathbb{T} \to \mathbb{R}^3$, where $\boldsymbol{F}(\sigma,t)$ is a vector in the world coordinate. Then the net internal force on the segment is described as

$$\boldsymbol{F}(\sigma+d\sigma,t)-\boldsymbol{F}(\sigma,t) \simeq \partial_\sigma \boldsymbol{F}(\sigma,t)d\sigma. \tag{24}$$

At both ends of the robot, the forces $\boldsymbol{F}(0,t)$ and $\boldsymbol{F}(L,t)$ are equal to zero.

The forces described above can have the component in the normal direction of the surface. Therefore, a constraint force distribution is necessary to keep the entire robot body on the surface. Let the normal force distribution be denoted by $N(\sigma,t)\boldsymbol{e}_n(\sigma,t)$, where N is a positive real-valued function from $[0,\, L]\times\mathbb{T}$ to $\mathbb{R}$. The vector $N(\sigma,t)d\sigma\boldsymbol{e}_n(\sigma,t)$ can be referred to as a normal reaction from the surface.

As in the existing studies [6,7], we assume that there exists an internal torque distribution $\boldsymbol{T} : [0,\, L]\times\mathbb{T}\to\mathbb{R}^3$ that can be used as the input of the robot.

The torques from the gravity, the friction, and the normal reaction are the second-order terms of $d\sigma$. By taking $d\sigma$ as a small number, these torques can be negligible. The torque from the internal force remains as the first-order term of $d\sigma$, as is shown in the study [6]. The torque term from the internal force is written as $\boldsymbol{e}_r(\sigma,t)\times\boldsymbol{F}(\sigma,t)d\sigma$.

From the discussion above, the forces acting on the small segment can be taken together into

$$\begin{aligned}&\boldsymbol{F}_{\text{seg}}(\sigma,t)d\sigma\\ &=(\rho\boldsymbol{g}+\partial_\sigma\boldsymbol{F}(\sigma,t)+N(\sigma,t)\boldsymbol{e}_n(\sigma,t)\\ &\quad -c_r v_r(\sigma,t)\boldsymbol{e}_r(\sigma,t)-c_b v_b(\sigma,t)\boldsymbol{e}_b(\sigma,t))d\sigma,\end{aligned} \tag{25}$$

and the torques are going to be

$$\begin{aligned}\boldsymbol{T}_{\text{seg}}(\sigma,t)d\sigma &= \boldsymbol{T}(\sigma+d\sigma,t)-\boldsymbol{T}(\sigma,t)\\ &\quad +\boldsymbol{e}_r(\sigma,t)\times\boldsymbol{F}(\sigma,t)d\sigma\\ &=(\partial_\sigma\boldsymbol{T}(\sigma,t)+\boldsymbol{e}_r(\sigma,t)\times\boldsymbol{F}(\sigma,t))\,d\sigma,\end{aligned} \tag{26}$$

where $\boldsymbol{F}_{\text{seg}}(\sigma,t)$ and $\boldsymbol{T}_{\text{seg}}(\sigma,t)$ are the force and torque distribution for the infinitesimal segment, respectively.

4.2. The equations of motion of the robot segment

As mentioned in Subsection 3.2, the essential variables of the robot locomotion are the translational velocity $v_r(\sigma,t)$, $v_b(\sigma,t)$, the rolling angular velocity $\omega_r(\sigma,t)$ and the yawing angular velocity $\omega_n(\sigma,t)$. The goal of the section is to derive the equations of motion for the four variables.

We put two assumptions on the inertia of the segment with length $d\sigma$. The shape of the segment is a cylinder of $d\sigma$ tall. The inertia matrix at the center of gravity is in the form of

$$I d\sigma = \text{diag}(I_r, I_b, I_b)d\sigma, \tag{27}$$

in the Darboux frame. Note that the backbone frame shares $\boldsymbol{e}_r(\sigma,t)$ with the Darboux frame. Therefore the inertia matrix is invariant with the transition between the two frames.

The equations of motion of the infinitesimal segment are described as follows:

$$\rho\partial_{tt}\boldsymbol{x}(\sigma,t) = \boldsymbol{F}_{\text{seg}}(\sigma,t), \tag{28}$$

$$I\partial_t\boldsymbol{\omega}_d(\sigma,t) = -\boldsymbol{\omega}_d(\sigma,t)\times I\boldsymbol{\omega}_d(\sigma,t)+\boldsymbol{T}_{\text{seg}}(\sigma,t). \tag{29}$$

The first and third entries of (29) are the equations of motion for $\omega_r(\sigma,t)$ and $\omega_n(\sigma,t)$, respectively. The inner products of (28) and $\boldsymbol{e}_r(\sigma,t)$, $\boldsymbol{e}_b(\sigma,t)$ give the equations of motion of the translation motion of the segment.

By differentiating the velocity constraint (6), the following equation is derived:

$$\begin{aligned}&\partial_{tt}\boldsymbol{x}(\sigma,t)\\ &=\partial_t v_r(\sigma,t)\boldsymbol{e}_r(\sigma,t)+\partial_t v_b(\sigma,t)\boldsymbol{e}_b(\sigma,t)\\ &\quad +v_r\partial_t\boldsymbol{e}_r(\sigma,t)+v_b\partial_t\boldsymbol{e}_b(\sigma,t)\\ &=(\partial_t v_r(\sigma,t)-v_b(\sigma,t)\tilde{\omega}_n(\sigma,t))\boldsymbol{e}_r(\sigma,t)\\ &\quad +(\partial_t v_b(\sigma,t)+v_r(\sigma,t)\tilde{\omega}_n(\sigma,t))\boldsymbol{e}_b(\sigma,t)\\ &\quad +(v_b(\sigma,t)\tilde{\omega}_r(\sigma,t)-v_r(\sigma,t)\omega_b(\sigma,t))\boldsymbol{e}_n(\sigma,t),\end{aligned} \tag{30}$$

where (20), (21), and

$$\partial_t\boldsymbol{e}_b(\sigma,t) = -\tilde{\omega}_n(\sigma,t)\boldsymbol{e}_r(\sigma,t)+\tilde{\omega}_r(\sigma,t)\boldsymbol{e}_n(\sigma,t) \tag{31}$$

are used. Calculating the inner products, the equations of motion are described as

$$\rho\partial_t v_r(\sigma,t) = v_b(\sigma,t)\omega_n(\sigma,t)+\boldsymbol{e}_r(\sigma,t)^T\boldsymbol{F}_{\text{seg}}(\sigma,t), \tag{32}$$

$$\rho\partial_t v_b(\sigma,t) = -v_r(\sigma,t)\omega_n(\sigma,t)+\boldsymbol{e}_b(\sigma,t)^T\boldsymbol{F}_{\text{seg}}(\sigma,t), \tag{33}$$

where $\tilde{\omega}_n(\sigma,t)$ is replaced by $\omega_n(\sigma,t)$ by using (21).

Equations (32) and (33) do not have the normal reaction term $N(\sigma,t)\boldsymbol{e}_n(\sigma,t)$. However, the right-hand sides of (32) and (33) still rely on the internal force normal to the surface, which can be checked as follows: Let the internal force be denoted as follows:

$$\begin{bmatrix}F_r(\sigma,t)\\ F_b(\sigma,t)\\ F_n(\sigma,t)\end{bmatrix} = R_d(\sigma,t)^T\boldsymbol{F}(\sigma,t). \tag{34}$$

Then, the net internal force term $\partial_\sigma\boldsymbol{F}(\sigma,t)$ in $\boldsymbol{F}_{\text{seg}}(\sigma,t)$ is written as

$$\begin{aligned}&\partial_\sigma\boldsymbol{F}(\sigma,t)\\ &=(\partial_\sigma F_r(\sigma,t)-\kappa_g(\sigma,t)F_b(\sigma,t)\end{aligned}$$

$$
\begin{aligned}
&-\kappa_n(\sigma,t)F_n(\sigma,t))\boldsymbol{e}_r(\sigma,t)\\
&+(\partial_\sigma F_b(\sigma,t)+\kappa_g(\sigma,t)F_r(\sigma,t)\\
&-\tau_g(\sigma,t)F_n(\sigma,t))\boldsymbol{e}_b(\sigma,t)\\
&+(\partial_\sigma F_n(\sigma,t)+\kappa_n(\sigma,t)F_r(\sigma,t)\\
&+\tau_g(\sigma,t)F_b(\sigma,t))\boldsymbol{e}_n(\sigma,t).
\end{aligned}
\tag{35}
$$

The force terms of (32) and (33) contain $\boldsymbol{e}_r(\sigma,t)^T\partial_\sigma\boldsymbol{F}(\sigma,t)$ and $\boldsymbol{e}_b(\sigma,t)^T\partial_\sigma\boldsymbol{F}(\sigma,t)$, respectively. Thus, the right-hand sides of (32) and (33) have the force terms $-\kappa_n(\sigma,t)F_n(\sigma,t)$ and $-\tau_g(\sigma,t)F_n(\sigma,t)$.

In the rest of this section, the goal is to get rid of $F_n(\sigma,t)$ from the right-hand sides of the equations of motion (32), (33). By the notation (34), the right-hand side of the second entry of (29) can be written as

$$
l_b(\sigma,t)+u_b(\sigma,t)-F_n(\sigma,t),
\tag{36}
$$

where $l_b(\sigma,t)$ and $u_b(\sigma,t)$ are defined as

$$
\begin{bmatrix} l_r(\sigma,t)\\ l_b(\sigma,t)\\ l_n(\sigma,t)\end{bmatrix}
=-\boldsymbol{\omega}_d(\sigma,t)\times I\boldsymbol{\omega}_d(\sigma,t),
\tag{37}
$$

$$
\begin{bmatrix} u_r(\sigma,t)\\ u_b(\sigma,t)\\ u_n(\sigma,t)\end{bmatrix}
=\partial_\sigma\boldsymbol{T}(\sigma,t).
\tag{38}
$$

The angular acceleration $\partial_t\omega_b(\sigma,t)$ in (29) can be expressed by $\partial_t v_r(\sigma,t)$ and $\partial_t v_b(\sigma,t)$ using the constraint (7)

$$
\begin{aligned}
&I_b\partial_t\omega_b(\sigma,t)\\
&=-I_b\kappa_n(\sigma,t)\partial_t v_r(\sigma,t)-I_b\tau_g(\sigma,t)\partial_t v_b(\sigma,t)\\
&\quad-I_b\partial_t\kappa_n(\sigma,t)v_r(\sigma,t)-I_b\partial_t\tau_g(\sigma,t)v_b(\sigma,t).
\end{aligned}
\tag{39}
$$

Therefore, by equating (36) and the right-hand side of (39),

$$
\begin{aligned}
&F_n(\sigma,t)\\
&=I_b\kappa_n(\sigma,t)\partial_t v_r(\sigma,t)+I_b\tau_g(\sigma,t)\partial_t v_b(\sigma,t)\\
&\quad+I_b\partial_t\kappa_n(\sigma,t)v_r(\sigma,t)+I_b\partial_t\tau_g(\sigma,t)v_b(\sigma,t)\\
&\quad+l_b(\sigma,t)+u_b(\sigma,t)
\end{aligned}
\tag{40}
$$

is obtained as an alternative expression for $F_n(\sigma,t)$.

Under the notation (34), the right-hand sides of (32) and (33) are rewritten as

$$
\begin{aligned}
&\rho\partial_t v_r(\sigma,t)\\
&=v_b(\sigma,t)\omega_n(\sigma,t)+\rho\boldsymbol{e}_r(\sigma,t)^T\boldsymbol{g}-c_r v_r(\sigma,t)\\
&\quad+\partial_\sigma F_r(\sigma,t)-\kappa_g(\sigma,t)F_b(\sigma,t)-\kappa_n(\sigma,t)F_n(\sigma,t),
\end{aligned}
\tag{41}
$$

$$
\begin{aligned}
&\rho\partial_t v_b(\sigma,t)\\
&=-v_r(\sigma,t)\omega_n(\sigma,t)+\rho\boldsymbol{e}_b(\sigma,t)^T\boldsymbol{g}-c_b v_b(\sigma,t)\\
&\quad+\partial_\sigma F_b(\sigma,t)+\kappa_g(\sigma,t)F_r(\sigma,t)-\tau_g(\sigma,t)F_n(\sigma,t).
\end{aligned}
\tag{42}
$$

By substituting the result of (40) for $F_n(\sigma,t)$ of (41) and (42), we have the following equation:

$$
\begin{aligned}
M(\sigma,t)\partial_t\boldsymbol{v}(\sigma,t)=&\begin{bmatrix}\partial_\sigma F_r(\sigma,t)\\ \partial_\sigma F_b(\sigma,t)\end{bmatrix}+K(\sigma,t)\begin{bmatrix}F_r(\sigma,t)\\ F_b(\sigma,t)\end{bmatrix}\\
&+\boldsymbol{\phi}(\sigma,t),
\end{aligned}
\tag{43}
$$

where the matrices $M(\sigma,t)$, $K(\sigma,t)$ and the vectors $\boldsymbol{v}(\sigma,t)$, $\boldsymbol{\phi}(\sigma,t)$ are defined as follows ((σ,t) is omitted):

$$
M=\begin{bmatrix}\rho+I_b\kappa_n^2 & I_b\tau_g\kappa_n\\ I_b\tau_g\kappa_n & \rho+I_b\tau_g^2\end{bmatrix},
\tag{44}
$$

$$
K=\begin{bmatrix}0 & -\kappa_g\\ \kappa_g & 0\end{bmatrix},
\tag{45}
$$

$$
\boldsymbol{v}=\begin{bmatrix}v_r\\ v_b\end{bmatrix},
\tag{46}
$$

$$
\boldsymbol{\phi}=-\boldsymbol{P}-C\begin{bmatrix}v_r\\ v_b\end{bmatrix},
\tag{47}
$$

$$
C=\begin{bmatrix}c_r+I_b\kappa_n\frac{\partial\kappa_n}{\partial t} & -\rho\omega_n+I_b\kappa_n\frac{\partial\tau_g}{\partial t}\\ \rho\omega_n+I_b\tau_g\frac{\partial\kappa_n}{\partial t} & c_b+I_b\tau_g\frac{\partial\tau_g}{\partial t}\end{bmatrix},
\tag{48}
$$

$$
\boldsymbol{P}=(l_b+u_b)\begin{bmatrix}\kappa_n\\ \tau_g\end{bmatrix}-\rho\begin{bmatrix}\boldsymbol{e}_r^T\\ \boldsymbol{e}_b^T\end{bmatrix}\boldsymbol{g}.
\tag{49}
$$

The first and third entries of (29), i.e.,

$$
I_r\partial_t\omega_r(\sigma,t)=l_r(\sigma,t)+u_r(\sigma,t),
\tag{50}
$$

$$
I_b\partial_t\omega_n(\sigma,t)=l_n(\sigma,t)+u_n(\sigma,t)+F_b(\sigma,t),
\tag{51}
$$

and (43) are the equations of motion on the surface and fully describe the locomotion of the robot.

4.3. The internal force distribution

As mentioned in Section 2, the previous studies [6,7] depend on the sideslip constraint or the periodicity of the body shape to handle the internal force distribution. Our model introduced in the previous section expresses a wider class of locomotion free from these restrictions. This difference calls for a new approach to the determination problem of the internal force.

We solve the problem as a boundary value problem for $F_r(\sigma,t)$ and $F_b(\sigma,t)$. The main goal of this section is to derive a second-order partial derivative equation from the equations of motion (43), (50), and (51). Note that we omit (σ,t) in this section, except when we introduce a new mapping.

The partial derivative of (43) with respect to σ is

$$
\partial_\sigma M\partial_t\boldsymbol{v}+M\partial_{\sigma t}\boldsymbol{v}
$$

$$= \partial_\sigma \boldsymbol{\phi} + \begin{bmatrix} \partial_{\sigma\sigma} F_r \\ \partial_{\sigma\sigma} F_b \end{bmatrix} + K \begin{bmatrix} \partial_\sigma F_r \\ \partial_\sigma F_b \end{bmatrix} + \partial_\sigma K \begin{bmatrix} F_r \\ F_b \end{bmatrix}. \quad (52)$$

The acceleration vector $\partial_t \boldsymbol{\nu}$ turns into the force terms that contain F_r and F_b by substituting the equation of motion (43) for $\partial_t \boldsymbol{\nu}$.

From (17), the vector $\partial_{\sigma t} \boldsymbol{x}$ equals $\omega_n \boldsymbol{e}_b - \omega_b \boldsymbol{e}_n$. By differentiating (6) with respect to σ, the vector $\partial_{\sigma t} \boldsymbol{x}$ can also be described by using v_r and v_b as

$$\begin{aligned} \partial_{\sigma t} \boldsymbol{x} = &(\partial_\sigma v_r - \kappa_g v_b) \boldsymbol{e}_r \\ &+ (\partial_\sigma v_b + \kappa_g v_r) \boldsymbol{e}_b \\ &+ (\kappa_n v_r + \tau_g v_b) \boldsymbol{e}_n. \end{aligned} \quad (53)$$

By comparing the entries of each direction, the following equation is derived

$$\partial_\sigma \boldsymbol{\nu} = -K\boldsymbol{\nu} + \begin{bmatrix} 0 \\ \omega_n \end{bmatrix}, \quad (54)$$

and its time-derivative is

$$\partial_{\sigma t} \boldsymbol{\nu} = -\partial_t K \boldsymbol{\nu} - K \partial_t \boldsymbol{\nu} + \begin{bmatrix} 0 \\ \partial_t \omega_n \end{bmatrix}. \quad (55)$$

The acceleration terms $\partial_t \boldsymbol{\nu}$ and $\partial_t \omega_n$ are rewritten using the equations of motion (43) and (51). Therefore, $\partial_{\sigma t} \boldsymbol{\nu}$ itself can be written using F_r and F_b.

The substitutions for $\partial_{\sigma t} \boldsymbol{\nu}$, $\partial_t \boldsymbol{\nu}$, and $\partial_t \omega_n$ in (52) result in

$$\begin{bmatrix} \partial_{\sigma\sigma} F_r \\ \partial_{\sigma\sigma} F_b \end{bmatrix} + \bar{D} \begin{bmatrix} \partial_\sigma F_r \\ \partial_\sigma F_b \end{bmatrix} + \bar{K} \begin{bmatrix} F_r \\ F_b \end{bmatrix} = \boldsymbol{f}, \quad (56)$$

where the matrices $\bar{D}(\sigma,t)$, $\bar{K}(\sigma,t)$, and the vector $\boldsymbol{f}(\sigma,t)$ are defined as follows:

$$\bar{D} = K - (\partial_\sigma M - MK), \quad (57)$$

$$\bar{K} = \partial_\sigma K - (\partial_\sigma M - MK) M^{-1} K - M \begin{bmatrix} 0 & 0 \\ 0 & I_b^{-1} \end{bmatrix}, \quad (58)$$

$$\begin{aligned} \boldsymbol{f} = &(\partial_\sigma M - MK) M^{-1} \boldsymbol{\phi} \\ &+ M \left(-\partial_t K \boldsymbol{\nu} + \begin{bmatrix} 0 \\ I_b^{-1}(l_n + u_n) \end{bmatrix} \right) - \partial_\sigma \boldsymbol{\phi}. \end{aligned} \quad (59)$$

Solving (56) under the condition $F_r(0,t) = F_r(L,t) = 0$, $F_b(0,t) = F_b(L,t) = 0$, the distribution of the internal forces can be obtained, and the time development of the locomotion can be calculated by the equations of motion (43), (50), and (51). Note that the geodesic torsion and curvature tell the change in the orientation of the body segment along the body curve. In the case of a multilink robot, the change in the orientation is expressed by the joint angles. In the sense that both tell the directional change, τ_g and κ_g correspond to the angle of the joints of a multilink snake-like robot, and $\partial_t \tau_g$ and $\partial_t \kappa_g$ are the joint angular velocities. Therefore, the vector $\boldsymbol{f}$ and the coefficient matrices $\bar{D}$, $\bar{K}$ are determined by the current robot state and the input.

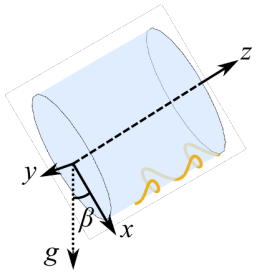

Fig. 4. The surface S (blue) and the desired curve (yellow).

5. CONTROLLER

As an application of our model, we developed simple controllers for the continuous snake-like robot based on the model. The control objectives are

1) to generate lateral undulation, and
2) to keep the belly touching the surface.

The first objective is a common method for generating thrust forces and forms the foundation for position controls on the surface. The second objective aims at creating another application for the robot; by letting the back away from the surface, the robot can carry luggage on the back.

The controller for the first objective is developed based on PD control. The actual input and the reference trajectory are shown in Subsection 5.1. The shape of the reference trajectory is environment specific. We restrict the surface to a cylinder as a simple example in this paper. However, the flow of the discussion remains the same for any smooth surface S.

Fig. 4 illustrates the shape of the cylinder, where β stands for the inclined angle against the gravitaty. Let the cylinder have a radius of R and its axis be the z-axis of $\mathbb{R}^3$. Denote a coordinate of a point in $\mathbb{R}^3$ by cylindrical coordinate system (R, θ_s, z) in which θ_s stands for the direction of the point and z is the height from the x-y plane. Then, one of the coordinate chart systems of the surface (denoted as S) of the cylinder is given as follows:

$$\phi([R,\ \theta_s,\ z]^T) = [z,\ R\theta_s]^T. \quad (60)$$

This map corresponds to opening up the cylinder, thus the local coordinate chart of ϕ covers the entire cylinder up.

We put an assumption on the internal torque $\boldsymbol{T}(\sigma,t)$. As the internal force distribution, the torque distribution $\boldsymbol{T}(\sigma,t)$ needs to equal zero at $\sigma = 0, L$. In this paper, we

remove the boundary condition to simplify the construction of the controller and take $[u_r, u_b, u_n]^T$ as the input of the system. A similar assumption was made in [7].

5.1. Serpentine locomotion generation

To generate lateral undulation, we follow the convention of a controller for multilink snake-like robots. The shift control [2] is one of the common methods to make the robot follow a smooth desired path. The method is based on the shape approximation of a curve by the links of the robot. When given a desired path as a curve in $\mathbb{R}^3$, the joint angles of the robot is determined to fit the body to a part of the curve. Then, by shifting the approximated part along the curve from moment to moment, the robot generates a motion that looks like the robot slithering along the curve. The shift control does not always ensure the strict path following of the robot because of the approximation. However, it is still useful to generate desired locomotion and is a popular method in gait design research [2,4,5].

When fitting the robot body to a curve in $\mathbb{R}^3$, there exists a degree of freedom of rolling. Thus, the desired curve is often given with the desired backbone frame on it. The way to determine the joint angles is as follows. Let the desired curve be denoted by $\hat{c} : s \in \mathbb{R} \mapsto \hat{c}(s) \in \mathbb{R}^3$, s be the arc-length parameter and $\{\hat{\boldsymbol{e}}_r(\sigma,t), \hat{\boldsymbol{e}}_p(\sigma,t), \hat{\boldsymbol{e}}_y(\sigma,t)\}$ be the desired backbone frame. We consider the case where the robot moves along $\hat{c}$ at reference speed $\hat{v}$ and the desired backbone frame meets the following equation:

$$\frac{d\hat{c}}{ds}(\sigma + \hat{v}t) = \hat{\boldsymbol{e}}_r(\sigma,t). \tag{61}$$

Then, the second derivative of $\hat{c}$ is written using some real-valued functions $\hat{\kappa}_p(\sigma,t)$ and $\hat{\kappa}_y(\sigma,t)$ as

$$\frac{d^2\hat{c}}{ds^2}(\sigma + \hat{v}t) = \hat{\kappa}_y(\sigma,t)\hat{\boldsymbol{e}}_p(\sigma,t) - \hat{\kappa}_p(\sigma,t)\hat{\boldsymbol{e}}_y(\sigma,t). \tag{62}$$

Regarding s as time, $\hat{\kappa}_p(\sigma,t)$ and $\hat{\kappa}_y(\sigma,t)$ correspond the angular velocities around the pitch axis and the yaw axis, respectively. In the geometrical sense, these functions tell how the direction of the body axis changes along the arc length. Thus, discretizing $\hat{\kappa}_y(\sigma,t)$ along σ gives the reference angles for the yaw joints (same for the pitch joints).

In the case of a flat plane, it is known that lateral undulation is generated by defining $\hat{c}$ such that

$$\hat{\kappa}_p(\sigma,t) = 0 \ (\forall(\sigma,t)), \tag{63}$$

$$\hat{\kappa}_y(\sigma,t) = \frac{2\pi}{T}\alpha \sin\left(\frac{2\pi}{T}(\sigma + \hat{v}t)\right), \tag{64}$$

where α and T are constant parameters [6]. The curve that satisfies (63) and (64) is often called the serpenoid curve.

A continuous snake-like robot can be regarded as a multilink snake-like robot consisting of links with infinitesimal length. Hence, $\hat{\kappa}_p(\sigma,t)$ and $\hat{\kappa}_y(\sigma,t)$ themselves can be seen as the reference joint angles. From the second control objective at the beginning of Section 5, the reference backbone frame is given as the one such that $\hat{\boldsymbol{e}}_y(\sigma,t) = \hat{\boldsymbol{e}}_n(\sigma,t)$ for all (σ,t), where $\{\hat{\boldsymbol{e}}_r(\sigma,t), \hat{\boldsymbol{e}}_b(\sigma,t), \hat{\boldsymbol{e}}_n(\sigma,t)\}$ be the Darboux frame on the desired curve. Thus, the main concern is how to give a concrete definition to $\hat{c}$ corresponding to "lateral undulation on a cylinder." We exploit the local coordinate chart to solve the problem.

The inverse of the local coordinate chart ϕ is a map from a plane to the surface of the cylinder. Therefore, ϕ^{-1} can paste the serpenoid curve on $\mathbb{R}^2$ to the surface S. Let the serpenoid curve on the plane be denoted by $\hat{c}_p(s)$ and satisfy the following conditions:

$$\hat{c}_p(0) = [0,\ 0]^T, \tag{65}$$

$$\frac{d\hat{c}_p}{ds}(0) = [\cos\alpha,\ \sin\alpha]^T. \tag{66}$$

Under the conditions, $\hat{c}_p(s)$ becomes an undulating curve centering its axis on the x-axis of $\mathbb{R}^2$. The map ϕ^{-1} is a smooth map, therefore, the mapped curve $\phi^{-1}(\hat{c}_p(s))$ remains smooth. The shape of $\phi^{-1}(\hat{c}_p(s))$ is shown as a yellow curve in Fig. 4. It does represent a lateral undulation on a cylinder. Hence, we take $\phi^{-1}(\hat{c}_p(s))$ as $\hat{c}(s)$ and end the definition of the reference curve.

In the case of a smooth snake-like robot on a curved surface S, the geometric curvature $\kappa_g(\sigma,t)$ represents the shape in the "lateral direction" of the surface, and u_n matters for the posture changing. Moreover, when the second control objective is achieved, i.e., when $\hat{\boldsymbol{e}}_p(\sigma,t) = \hat{\boldsymbol{e}}_b(\sigma,t)$ holds, the following equations hold

$$\begin{aligned}\hat{\kappa}_y(\sigma,t) &= \hat{\boldsymbol{e}}_p(\sigma,t)^T \frac{d^2c}{ds^2}(\sigma + vt) \\ &= \hat{\boldsymbol{e}}_b(\sigma,t)^T \frac{\partial \hat{\boldsymbol{e}}_r}{\partial \sigma}(\sigma,t) \\ &= \hat{\kappa}_g(\sigma,t).\end{aligned} \tag{67}$$

Thus, we take $\hat{\kappa}_y$ as the reference geometric curvature for the robot and construct the controller as

$$\begin{aligned}u_n(\sigma,t) = {} & k_p\left(\hat{\kappa}_y(\sigma,t) - \kappa_y(\sigma,t)\right) \\ & + k_d\left(\partial_t\hat{\kappa}_y(\sigma,t) - \partial_t\kappa_y(\sigma,t)\right),\end{aligned} \tag{68}$$

where k_p and k_d are positive constants.

5.2. Back side controller

As shown in Fig. 3, the rolling angle on the surface is given as $\theta(\sigma,t)$. The control objective 2 stands for achieving $\theta(\sigma,t) \to 0$ as t to ∞ for all σ. By looking $\theta(\sigma,t)$ as a function of σ parameterized by t, the objective is also interpreted as the convergence of the function into the zero function $0(\sigma)$. We introduce a backstepping-like controller and show the convergence of $\theta(\sigma,t)$ in the space of functions of σ. First, let us explain the time development of $\theta(\sigma,t)$ and some information that the controller uses.

The time derivative of $\theta(\sigma,t)$ equals the difference in the rolling speed between the segment and the Darboux frame on it. Thus the time-derivative of $\theta(\sigma,t)$ can be expressed as

$$\partial_t\theta(\sigma,t) = \tilde{\omega}_r(\sigma,t) - \omega_r(\sigma,t). \tag{69}$$

Note that the rolling speed $\tilde{\omega}_r(\sigma,t)$ can be acquired from the equation

$$\tilde{\omega}_r(\sigma,t) = \boldsymbol{e}_b(\sigma,t)^T \partial_t \boldsymbol{e}_n(\sigma,t). \tag{70}$$

In the known surface, the value of $\partial_t\boldsymbol{e}_n(\sigma,t)$ is available by differentiating the definition of $\boldsymbol{e}_n$ (2). Therefore, the value can be used to calculate the control input. Moreover, the equations of motion for the translational movement (43) and the rolling (50) are independent of each other, which enables us to calculate the time-derivative of $\tilde{\omega}_r(\sigma,t)$ from the state of the system of the robot.

From the notation above, let us introduce a controller using the information of $\tilde{\omega}_r(\sigma,t)$ and $\partial_t\tilde{\omega}_r(\sigma,t)$. First, let us assume that $\omega_r(\sigma,t)$ can be used as an input for (69). Then, setting $\omega_r(\sigma,t)$ as

$$\omega_r(\sigma,t) = \tilde{\omega}_r(\sigma,t) + k_1\theta(\sigma,t) \quad (k_1 > 0), \tag{71}$$

achieves the convergence of $\theta(\sigma,t)$ to 0 for a fixed σ. As an ordinary construction of a backstepping controller, apply the following transformation to (69) and the equation of motion of rolling (50)

$$\zeta(\sigma,t) = \omega_r(\sigma,t) - (\tilde{\omega}_r(\sigma,t) + k_1\theta(\sigma,t)). \tag{72}$$

That yields the transformed system

$$\begin{aligned}
\partial_t\theta(\sigma,t) &= \tilde{\omega}_r(\sigma,t) - \omega_r(\sigma,t),\\
\partial_t\zeta(\sigma,t) &= J_r^{-1}(l_r(\sigma,t) + u_r(\sigma,t))\\
&\quad - (\partial_t\tilde{\omega}_r(\sigma,t) + k_1\partial_t\theta(\sigma,t)).
\end{aligned} \tag{73}$$

Then, the following proposition holds.

Proposition 2: Setting the control input $u_r(\sigma,t)$ as

$$\begin{aligned}
u_r(\sigma,t) &= J_r(\theta(\sigma,t) - k_2\zeta(\sigma,t)) - l_r(\sigma,t)\\
&\quad + \partial_t(\tilde{\omega}_r(\sigma,t) + k_1\theta(\sigma,t)),
\end{aligned} \tag{74}$$

makes $\theta(\sigma,t)$ converge to 0 for all σ.

Proof: Applying the controller (74) to the system (73) yields the following closed-loop system:

$$\partial_t\theta(\sigma,t) = -k_1\theta(\sigma,t) - \zeta(\sigma,t), \tag{75}$$
$$\partial_t\zeta(\sigma,t) = \theta(\sigma,t) - k_2\zeta(\sigma,t). \tag{76}$$

Let a non-negative-valued function V be defined as

$$V(t) = \int_0^L \frac{1}{2}\left(\theta(\sigma,t)^2 + \zeta(\sigma,t)^2\right) d\sigma. \tag{77}$$

This gives the square of the distance between the vector value function $[\theta(\sigma,t),\ \zeta(\sigma,t)]^T$ and the zero function $[0(\sigma),\ 0(\sigma)]^T$. Note that, when $\theta(\sigma,t),\ \zeta(\sigma,t) \neq 0(\sigma)$, the time derivation of V always takes a negative value as

$$\begin{aligned}
\dot{V}(t) &= \frac{d}{dt}\left(\int_0^L \frac{1}{2}\left(\theta(\sigma,t)^2 + \zeta(\sigma,t)^2\right) d\sigma\right)\\
&= \int_0^L \frac{\partial}{\partial t}\left(\frac{1}{2}\left(\theta(\sigma,t)^2 + \zeta(\sigma,t)^2\right)\right) d\sigma\\
&= \int_0^L (\theta(\sigma,t)\partial_t\theta(\sigma,t) + \zeta(\sigma,t)\partial_t\zeta(\sigma,t))\, d\sigma\\
&= \int_0^L \left(-k_1\theta(\sigma,t)^2 - k_2\zeta(\sigma,t)^2\right) d\sigma < 0.
\end{aligned} \tag{78}$$

Therefore, we now know that there exists a non-negative value V^* such that $V(t) \to V^*$ as $t \to \infty$.

Our remaining concern is whether $V^* = 0$ or not. Note that, if $\dot{V}(t) \to 0$ holds, we can conclude that $V^* = 0$. From (75) and (76), $\partial_t\theta$ and $\partial_t\zeta$ are the zero function if and only if θ and ζ are the zero function. Therefore, under the assumption $\dot{V}(t) \to 0$, V^* cannot be non-zero.

From the above discussion, showing the conversion of $\dot{V}(t)$ to zero ends this proof. We have already proven that $V(t)$ converges to some value. Thus, from Barbalat's lemma, showing the boundedness of $\ddot{V}(t)$ concludes that $\dot{V}(t) \to 0$.

Define $\bar{k}$ as $\max\{k_1,\ k_2\}$. The absolute value of $\ddot{V}(t)$ satisfies the following inequation (we omitted (σ,t). All θ and ζ in (79) must be considered as $\theta(\sigma,t)$ and $\zeta(\sigma,t)$, respectively):

$$\begin{aligned}
&\|\ddot{V}(t)\|\\
&= \left\|\int_0^L \left(2k_1^2\theta^2 + 2k_2^2\zeta^2 + 2(k_1-k_2)\theta\zeta\right) d\sigma\right\|\\
&\leq \left\|\int_0^L (2k_1^2\theta^2 + 2k_2^2\zeta^2 + (k_1-k_2)(\theta^2+\zeta^2))d\sigma\right\|\\
&\leq \left\|\int_0^L (2\bar{k}^2\theta^2 + 2\bar{k}\zeta^2 + \bar{k}(\theta^2+\zeta^2))d\sigma\right\|\\
&= \left\|2(2\bar{k}^2+\bar{k})V(t)\right\|\\
&\leq \left\|2(2\bar{k}^2+\bar{k})V(0)\right\| = \text{const.}
\end{aligned} \tag{79}$$

From (79), it is shown that $\ddot{V}(t)$ is bounded. Therefore, we conclude that $V^* = 0$ and $\theta(\sigma,t)$ and $\zeta(\sigma,t)$ converge to the zero function. □

5.3. The remaining input

The remaining input $u_b(\sigma,t)$ affects the internal force $F_n(\sigma,t)$ and the normal reaction $N(\sigma,t)$. Proper $u_b(\sigma,t)$ can restrain the internal force or enhance the reaction from the surface.

In this paper, we use $u_b(\sigma,t)$ to force $F_n(\sigma,t)$ to be zero. Real-world snake-like robots often suffer from fastening failure of links due to the forces between them. Under this control, a reduction in the failure rate of the robots can be

expected. In addition, the reduction of the internal forces helps to enhance the calculation stability.

The force control is achieved by the following input:

$$\begin{aligned} u_b(\sigma,t) = &-l_b(\sigma,t) + F_{nr}(\sigma,t) \\ &- J_b \partial_t \kappa_n(\sigma,t) v_r(\sigma,t) - J_b k n(\sigma,t) \partial_t v_r(\sigma,t) \\ &- J_b \partial_t \tau_g(\sigma,t) v_b(\sigma,t) - J_b \tau_g(\sigma,t) \partial_t v_b(\sigma,t), \end{aligned} \tag{80}$$

where $F_{nr}(\sigma,t)$ is a reference distribution of $F_n(\sigma,t)$ satisfying $F_{nr}(0,t) = F_{nr}(L,t) = 0$. The controller needs information on translational acceleration. In practical cases, a snake-like robot often equips an IMU or an AHRS sensor for observation of the orientation of the robot. These sensors give real-time acceleration data, therefore the acceleration feedback is feasible. We set $F_{nr}(\sigma,t)$ as a constant value function zero.

6. SIMULATION

We carried out numerical simulation for the continuous snake-like robot based on the dynamical model developed in Section 4. As mentioned in Section 5, the terrain was the surface of the cylinder shown in Fig. 4. The inclined angle β was 30°, and the radius was 1 m. The parameters of the robot and the controller are shown in Table 1. We examined our model in the two cases with different frictional coefficients. In the first simulation (Simulation 1), c_r is set as 0.1 N/s. In the second simulation (Simulation 2), c_r is 0.01 N/s. Note that we added the term $-10\omega_n(\sigma,t)$ to $u_n(\sigma,t)$ of (68). The term was introduced to enhance the computational stability of numerical simulation. By the existence of this term, the amplitude of the undulation may get smaller than the one without the term. However, as shown in the results in this section, the proportional term and the derivative term of the PD controller were strong enough that the robot could ascend an inclined cylinder. Therefore, the term is negligible on the thrust generation.

Table 1. The parameters of the robot and the controller. ○: used in Simulation 1. ∗: used in Simulation 2.

Robot		Controller	
L	1 m	k_p	1
ρ	1 kg/m	k_d	2
J_r	0.32 kg·m^2	k_1	5
J_b	0.16 kg·m^2	k_2	5
c_r	0.1 N/s ○	$2\pi\alpha/T$	4.93
	0.01 N/s ∗	$2\pi/T$	6.28
c_b	40 N/s	v	1.5

6.1. Simulation 1

Fig. 5 shows the movement of the robot at $t = 0$, 5, 10 s. The initial position of the tail end was located at $z = 0$. At $t = 10$, the position was at about $z = 1$. Therefore, the robot achieved a one-meter displacement on the inclined cylinder.

Fig. 6 is the view from the top of the cylinder at the corresponding time. The orange arrows represent $\boldsymbol{e}_y(\sigma,t)$ and are normal to the surface of the cylinder, which means the back side controller worked well.

Figs. 7(a) and 7(b) illustrate the distribution of $F_r(\sigma,t)$ and $F_b(\sigma,t)$. In each of the graphs, the blue line shows the distribution at $t = 0$ s, the orange + chain line, and the yellow dotted line show the ones at $t = 5$ s and $t = 10$ s, respectively. From Fig. 7(b), it can be seen that the distribution of F_b forms a curve like a trigonometric function, which agrees with the analysis in Yamada and Hirose [6]. However, their analysis also expects trigonometric function-like distribution for F_r, which is not observed in our case, especially at $t = 5$ and 10 s. The possible cause of the disagreement is the inclination of the cylinder. The lower body (small σ side) needed to support the upper body during the locomotion, thus the lower segments

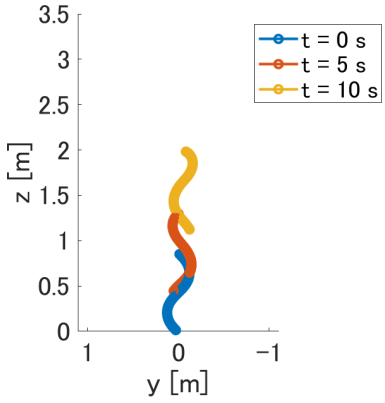

Fig. 5. The result of Simulation 1.

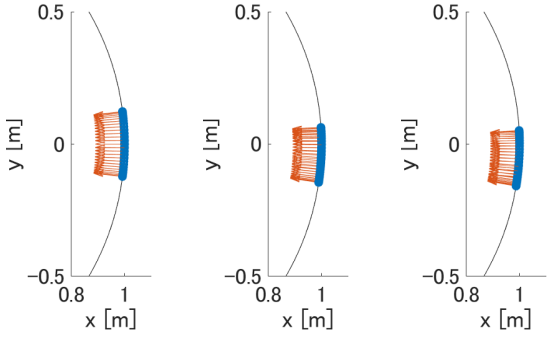

(a) $t = 0$ s. (b) $t = 5$ s. (c) $t = 10$ s.

Fig. 6. The direction of the back of the robot.

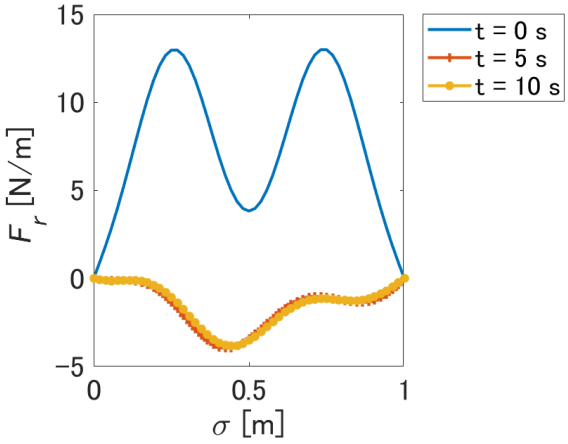

(a) The distribution of F_r.

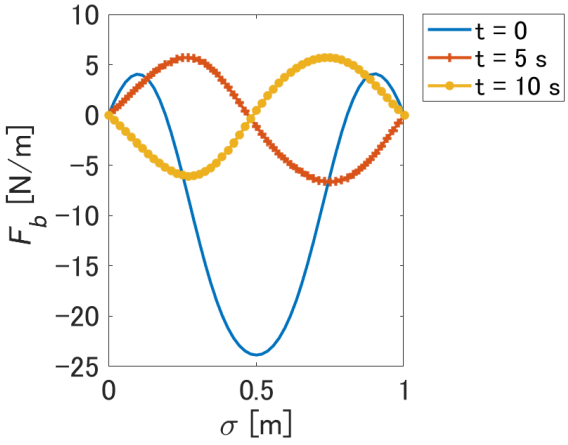

(b) The distribution of F_b.

Fig. 7. The internal forces at $t = 0$, 5, 10 s.

might tend to be more stressed than the upper ones. In fact, the peaks of the $F_r(\sigma,t)$ in Fig. 7(a) are on the smaller side of σ. The analysis in [6] depended on the infinite length of the robot and the periodic shape of the body curve. We conclude that our distribution is more likely in the case of this situation.

6.2. Simulation 2

Fig. 8 is the result when the tangential friction coefficient c_r is 0.01 N/s. As the figure shows, the robot slides down the cylinder due to the lack of frictional force. Note that, with the assumption of no sideslip, the robot slides down only when it takes the same shape as a geodesic of the surface, and the curvature and the torsion of the geodesic are constant in the neighborhood of the robot. In our simulation environment, slips can be observed only when the robot takes a straight line shape or a helix shape. Thus, using the previous models, even this simple phenomenon cannot be examined.

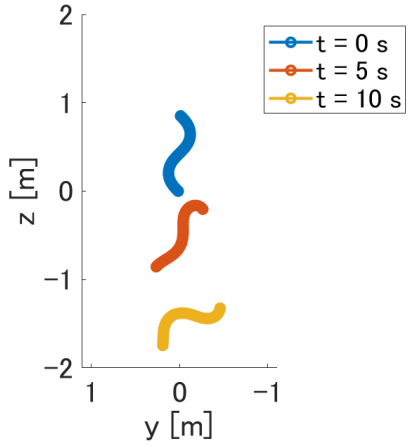

Fig. 8. The result of Simulation 2

In addition, the result gives important insight into the construction of snake-like robots. The tangential friction is considered as a nuisance and sometimes is ignored to simplify kinematic models [7]. However, the result reveals that the tangential friction has a crucial role to prevent the robots from sliding down curved surfaces.

Therefore, snake-like robots face the trade-off between energy efficiency and anti-slide performance. The lower tangential friction reduces the battery consumption and extends the uptime of the robots. However, greater friction extends the reachable area of the robots. Moreover, in the case of wheeled snake-like robots, using low-quality bearings for the wheels will achieve both high friction and a reduction of the cost of the robots at the same time. Therefore, tuning the tangential friction up will influence even the production of the snake-like robots.

7. CONCLUSION

In this paper, we introduced the new dynamical model and the controllers for a continuous snake-like robot. By using our model, the locomotion of the continuous snake-like robot can be examined even when it sideslips and even when it is on a curved surface. Our contribution serves to design controllers for locomotion in practically important environments, such as a slippery rock.

Furthermore, the simulation results revealed the important role of tangential friction which is underestimated in the previous studies. The tangential friction serves to prevent the robot from sliding down the surface, which is not trivial from models on horizontal plane terrain and from ones that ignore the sideslips of the robot. Moreover, the result yielded a notion of the trade-off relation between the energy efficiency and the reachability of the robot. The greater tangential drag will impact the battery consumption, however, in the case of snake-like robots, the drag expands the area where the robot can reach. The notion

will even illuminate using low-quality parts and can guide the production strategy of the snake-like robots.

We set the control of a real-world snake-like robot based on our model as our future work. The control input conversion from the smooth curve model into a multilink robot will also be handled.

CONFLICT OF INTEREST

The authors declare that there is no competing financial interest or personal relationship that could have appeared to influence the work reported in this paper. Shunichi Azuma is a Senior Editor of International Journal of Control, Automation, and Systems. Senior Editor status has no bearing on editorial consideration.

REFERENCES

[1] B. Li, L. Chen, and Y. Lv, "Development of a snake-like robot adapting to the ground," *Proc. of 8th Control, Automation, Robotics and Vision Conference (ICARCV 2004)*, vol. 1, pp. 273-277, 2004.

[2] T. Takemori, M. Tanaka, and F. Matsuno, "Gait design of a snake robot by connecting simple shapes," *Proc. of 2016 IEEE International Symposium on Safety, Security, and Rescue Robotics (SSRR)*, pp. 189-194, 2016.

[3] J. W. Burdick and J. Radford, "A 'sidewinding' locomotion gait for hyper-redundant robots," *Advanced Robotics*, vol. 9, no. 3, pp. 195-216, 1994.

[4] T. Kamegawa, T. Harada, and A. Gofuku, "Realization of cylinder climbing locomotion with helical form by a snake robot with passive wheels," *Proc. of 2009 IEEE International Conference on Robotics and Automation*, pp. 3067-3072, 2009.

[5] R. L. Hatton and H. Choset, "Generating gaits for snake robots: Annealed chain fitting and keyframe wave extraction," *Autonomous Robot*, vol. 28, pp. 271-281, 2010.

[6] H. Yamada and S. Hirose, "Study of active cord mechanism," *Journal of the Robotics Society of Japan*, vol. 26, no. 7, pp. 801-811, 2008.

[7] H. Date and Y. Takita, "Control of 3D snake-like locomotive mechanism based on continuum modeling," *Proc. of the ASME 2005 International Design Engineering Technical Conferences and Computers and Information in Engineering Conference. Volume 6: 5th International Conference on Multibody Systems, Nonlinear Dynamics, and Control, Parts A, B, and C*, vol. 6, pp. 1351-1359, 2005.

[8] J. Ha, "Robotic snake locomotion exploiting body compliance and uniform body tensions," *IEEE Transactions on Robotics*, vol. 39, no. 5, pp. 3875-3885, 2023.

[9] M. Travers, J. Whitman, P. Schiebel, D. Goldman, and H. Choset, "Shape-based compliance in locomotion," *Proc. of Robotics: Science and Systems 2016*, vol. 12, 2016.

[10] D. Rollinson, K. V. Alwala, N. Zevallos, and H. Choset, "Torque control strategies for snake robots," *Proc. of 2014 IEEE/RSJ International Conference on Intelligent Robots and Systems*, pp.1093-1099, 2014.

[11] H. Mochiyama, "The elastic rod approach toward system theory for soft robotics," *IFAC-PapersOnLine*, vol. 53, no. 2, pp. 9175-9180, 2020.

[12] L. Xun, G. Zheng, and A. Kruszewski, "Cosserat-rod-based Ddynamic modeling of soft slender robot interacting with environment," *IEEE Transactions on Robotics*, vol. 40, pp. 2811-2830, 2024.

[13] M. Gazzola, L. H. Dudte, A. G. McCormick, and L. Mahadevan, "Forward and inverse problems in the mechanics of soft filaments," *Royal Society Open Science*, vol. 5, no. 6, 2018.

[14] X. Zhang, F. K. Chan, T. Parthasarathy, and M. Gazzola, "Modeling and simulation of complex dynamic musculoskeletal architectures," *Nature Communications*, vol. 10, no. 1, 2019.

[15] J. Ostrowski and J. Burdick, "Gait kinematics for a serpentine robot," *Proc. of IEEE International Conference on Robotics and Automation*, vol. 2, pp. 1294-1299, 1996.

[16] P. Prautsch, T. Mita, and T. Iwasaki, "Analysis and control of a gait of snake robot", *IEEJ Transactions on Industry Applications*, vol. 120, no. 3, pp. 372-381, 2000.

[17] F. Matsuno and K. Mogi, "Control and unit design of redundant snake robots based on kinematic model," *Transactions of the Society of Instrument and Control Engineers*, vol. 36, no. 12, pp. 1108-1116, 2000.

[18] S. Ma, "Analysis of creeping locomotion of a snake-like robot," *Advanced Robotics*, vol. 15, no. 2, pp. 205-224, 2001.

[19] P. Liljeback, K. Y. Pettersen, Ø. Stavdahl, and J. T. Gravdahl, "Controllability and stability analysis of planar snake robot locomotion," *IEEE Transactions on Automatic Control*, vol. 56, no. 6, pp. 1365-1380, 2011.

[20] R. Ariizumi and F. Matsuno, "Dynamic analysis of three snake robot gaits," *IEEE Transactions on Robotics*, vol. 33, no. 5, pp. 1075-1087, 2017.

[21] M. Sato, M. Fukaya, and T. Iwasaki, "Serpentine locomotion with robotic snakes," *IEEE Control Systems Magazine*, vol. 22, no. 1, pp. 64-81, 2002.

[22] K. Harada, R. Ariizumi, M. Tanaka, T. Asai, and S. Azuma, "Head trajectory tracking control of an extendable snake-like robot," *Artificial Life and Robotics*, vol. 27, no.2, pp.316-323, 2022.

Koki Harada received his B.E. and M.E. degrees from Nagoya University in 2020, and 2022, respectively. His research interests include bio-inspired robots, space robots, and nonlinear control. He received the Student Presentation Award (SCI '24) in 2024. Mr. Harada is a member of IEEE, SICE, and ISCIE

Ryo Ariizumi received his B.E., M.E., and Ph.D. degrees from Kyoto University, Kyoto, Japan, in 2010, 2012, and 2015, respectively. He was a research fellow of the Japan Society for the Promotion of Science from 2014 to 2015 and an assistant professor at Nagoya University from 2015 to 2023. He is currently an associate professor at the Tokyo University of Agriculture and Technology. His research interests include the control of redundant robots and the optimization of robotic systems. He received the IEEE Robotics and Automation Society Japan Chapter Young Award (IROS2014) in 2014 and the Best Paper Award from the Robotics Society of Japan (RSJ) in 2018.

Toru Asai received his B.E., M.E., and Ph.D. degrees from Tokyo Institute of Technology, Japan, in 1991, 1993, and 1996, respectively. He has worked as a Research Fellow of JSPS between 1996 and 1998. In 1999, he joined the faculty of Osaka University. He was an Associate Professor of the sub-department of Mechatronics between 2015 and 2016 and the Department of Mechanical Systems Engineering between 2017 and 2023, Nagoya University. He is currently a professor of the Department of Mechanical Engineering, Chubu University, since 2024. His research interests include robust control, switching control, parameter estimation, and industrial applications. Dr. Asai is a member of IEEE, SICE, ISIJ, and ISCIE.

Shun-ichi Azuma received his B.E. degree in electrical engineering from Hiroshima University, Higashihiroshima, Japan, in 1999, and his M.E. and Ph.D. degrees in control engineering from the Tokyo Institute of Technology, Tokyo, in 2001 and 2004, respectively. He was an Assistant Professor with the Graduate School of Informatics, Kyoto University, Uji, Japan, from 2005, and an Associate Professor from 2011. From 2017 to 2022, he was a Professor with the Graduate School of Engineering, Nagoya University, Nagoya, Japan. He is currently a Professor with the Graduate School of Informatics, Kyoto University. His research interests include the analysis and control of hybrid systems. Dr. Azuma was an Associate Editor for the IEEE Transactions on Control of Network Systems from 2013 to 2019, and has been an Associate Editor for the IEEE CSS Conference Editorial Board since 2011, IFAC Journal Automatica since 2014, Nonlinear Analysis: Hybrid Systems since 2017, and IEEE Transactions on Automatic Control since 2019. He was a Research Fellow of the Japan Society for the Promotion of Science from 2004 to 2005.